RSC Advances

RSC Advances RSCPublishing

PAPER

Synergistically Thermodynamic and Kinetic Tailoring of the Hydrogen Desorption Properties of MgH_2 by Co-Addition of AlH_3 and CeF_3†

Cite this: DOI: 10.1039/x0xx00000x

Received
Accepted

DOI: 10.1039/x0xx00000x

www.rsc.org/advances

Haizhen Liu,[a] Chen Wu,[*,a] He Zhou[a], Tian Chen[a], Yongan Liu[a], Xinhua Wang[*,a,c], Zhaohui Dong[b], Hongwei Ge[a], Shouquan Li[c], and Mi Yan[a]

MgH_2 possesses a high hydrogen capacity and excellent reversibility. However, the high thermal stability and slow sorption kinetics retard its practical application as an on-board hydrogen storage material. In this work, AlH_3 and CeF_3 were introduced into the Mg-based material for the purpose of improving both the thermodynamic and the kinetic properties of MgH_2. DSC−TG analysis show that the onset hydrogen desorption temperature of MgH_2 can be synergistically reduced by 86 °C through co-addition of $0.25AlH_3$ and $0.01CeF_3$. Isothermal desorption measurements demonstrate that the co-addition of AlH_3 and CeF_3 significantly enhances the hydrogen desorption kinetics of MgH_2, with the absence of the induction period in the initial stage and the acceleration of hydrogen desorption process. In addition, this co-doped MgH_2 shows very good cycling stability at 300 °C, with a 1-h capacity of 3.5 wt% and a 3-h capacity of 4.5 wt%. Structure analysis by XRD measurements indicate that during the hydrogen desorption process, MgH_2 may react with Al (generated from the *in situ* decomposition of AlH_3) to form Mg solid solution and $Mg_{17}Al_{12}$, which contributes to the thermodynamic improvement of the Mg-based material. Besides, MgH_2 may also react with CeF_3 to form MgF_2 and $CeH_{2\sim3}$, which act both as the hydrogen diffusion gateways and as the impediment to the grain growth of MgH_2 during hydrogen sorption cycling, thus improving the hydrogen desorption kinetics and the cycling stability of MgH_2. Finally, it was found that the presence of AlH_3 will kinetically help CeF_3 to take its positive effect on the hydrogen desorption properties of MgH_2. This work provides a method for simultaneously tailoring the thermodynamic and the kinetic properties of MgH_2 by synergistic addition of metal hydride and rare earth fluoride.

1 Introduction

Magnesium hydride (MgH_2) is a promising candidate as a hydrogen storage material for on-board applications due to its high hydrogen capacity and excellent reversibility.[1] However, the unfavourably high thermodynamic stability and sluggish hydrogen sorption kinetics restrict the practical application of MgH_2.[2, 3]

To overcome the problems, mixing or alloying MgH_2/Mg with metals is one of the strategies.[4-14] Among the various metals, the metallic aluminium (Al) has been studied to improve the hydrogen sorption properties of MgH_2.[5, 7, 15, 16] Zaluska *et al.*[17] suggested that Al may not only act as a heat-transfer medium but also involve in the hydrogen sorption reactions of MgH_2. In our previous work[18, 19], we utilized aluminium hydride (AlH_3) as an Al source, replacing the metallic Al, to have significantly reduced the hydrogen desorption temperature of MgH_2. It was demonstrated that in the Mg−Al−H system, AlH_3 is much better than the metallic Al regarding its ability to improve the hydrogen desorption properties of MgH_2. It was suggested this superiority is ascribed not only to the brittleness feature of AlH_3, but also to the fact that AlH_3 will undergo the decomposition to form oxide-free Al* upon heating. The brittleness feature makes it easier for AlH_3 to mix with MgH_2 well to ensure uniform elemental distributions by short-term milling. The oxide-free Al* may benefit the reaction kinetics since it is of high chemical activity. However, the hydrogen desorption kinetics of the Mg−Al−H system suffers from severe decline when subjected to cycling.[20] It was indicated that this decline of kinetics is due to grain growth or particle agglomeration during the hydrogen sorption process.

Mixing with transition metal halides is another strategy that has been employed to successfully improve the hydrogen sorption kinetics of Mg-based materials.[21-29] It was suggested that many halides may react with MgH_2 and the product will act as impediment to the grain growth of MgH_2, thus improving the kinetics of MgH_2. However, while these metal halides can affect the kinetics of MgH_2, the thermodynamics of MgH_2 was barely changed. It is true that an improved kinetics is essential for fast hydrogen uptake and release, but the thermodynamic destabilization of MgH_2 is also highly desired because a lower stability means MgH_2 is able to start releasing hydrogen at a lower temperature.

In the present work, for the purpose of simultaneous thermodynamic and kinetic enhancement of MgH_2, the AlH_3 and a transition metal fluoride, cerium fluoride (CeF_3), were introduced together into the Mg-based materials by ball milling, with AlH_3 as the destabilizing agent and CeF_3 as the accelerating agent. The following will show that AlH_3 can thermodynamically destabilize

MgH_2, while CeF_3 can kinetically accelerate the hydrogen releasing. In addition, it is interesting that with co-addition of AlH_3 and CeF_3, the desorption properties of MgH_2 can be synergistically enhanced and this co-doped MgH_2 shows fast desorption kinetics and very good cycling stability at 300 °C. Moreover, CeF_3 was reported by Jin *et al.*[21] to have little influence on the hydrogen desorption of MgH_2. However, in the present work CeF_3 was found to be able to significantly reduce the desorption temperature of MgH_2, especially in the presence of a small amount of AlH_3.

2 Experimental Sections

Experimentally, MgH_2 (Alfa Aesar, 98%) and CeF_3 (Sinopharm Group, 99.9%) were used as-received and AlH_3 was synthesized by a wet chemical method[30-32]. Then the samples were prepared by ball milling the starting materials using a QM-3SP4 planetary mill (Nanjing Nanda Instrument Plant). In general, 1 g of powders and 50 g of stainless steel balls were sealed in a stainless steel vial with a volume of 100 mL. The milling was carried out at 400 rpm for 30 min. All handlings were operated under inert atmosphere. Four samples, *i.e.*, MgH_2, MgH_2 + $0.25AlH_3$, MgH_2 + $0.01CeF_3$, and MgH_2 + $0.25AlH_3$ + $0.01CeF_3$, were prepared for comparison. Then two series of samples, (that is, MgH_2 + $m$$CeF_3$ (m = 0.01, 0.02, and 0.05) and MgH_2 + $0.1AlH_3$ + $n$$CeF_3$ (n = 0.01, 0.02, and 0.05)), were prepared for further study.

Phase structures were determined by powder X-ray diffraction (XRD) using a PANalytical X-ray diffractometer (X'Pert Pro) with Cu Kα radiation. During sample transferring or measurement, the samples were sealed with amorphous membranes to avoid exposure to the air.

Nonisothermal hydrogen desorptions were studied by differential scanning calorimeter (DSC) and thermogravimetry (TG) analysis (Netzsch, STA449F3). The samples were heated from room temperature to 500 °C with a heating rate of 10 °C/min. During the heating process, flowing argon of 50 mL/min was utilized to prevent sample oxidation.

Isothermal desorptions were carried out on a lab-built Sieverts-type apparatus. Before the desorption measurement, the sample holder was evacuated to vacuum. Then the samples were rapidly heated to 300 °C and held at this temperature, during which the desorption curves were collected. Prior to the next desorption cycle, the dehydrogenated sample was rehydrogenated at 300 °C and 5 MPa H_2 for 1 h.

Field emission scanning electronic microscopy (SEM, FEI SU 70) was used to study the morphology of the samples.

3 Results and Discussion

The XRD patterns of the as-synthesized AlH_3 and the as-milled samples, shown in Fig. S1 (ESI†), indicate they are mainly the physical mixtures of the starting materials after milling. No CeF_3-relevant phases are detected in the CeF_3-doped samples, which may due to the low addition content.

Fig. 1 contains the DSC curves of the samples with a heating rate of 10 °C/min. As is seen from the DSC curves, the peak desorption temperature of the as-milled MgH_2 is 388 °C and is reduced to 375 (or 354 °C) when it is mixed with $0.25AlH_3$ (or $0.01CeF_3$). Then further reduction to 346 °C can be achieved by co-addition of $0.25AlH_3$ and $0.01CeF_3$, which means a synergistic enhancement effect.

Fig. 2 shows the TG curves of the samples. The weight loss of each sample during heating is indicated in the figure with the theoretical weight loss included in the parenthesis. The onset desorption temperature of the as-milled MgH_2 is 350 °C, which is reduced to 292 °C (or 301 °C) when it is mixed with $0.25AlH_3$ (or $0.01CeF_3$). Further reduction of the onset desorption temperature to 264 °C can be achieved by co-addition of $0.25AlH_3$ and $0.01CeF_3$. This desorption temperature of the co-doped MgH_2 is 86 °C lower than the as-milled MgH_2. Similar to the DSC results, the onset desorption temperature of the co-doped MgH_2 is the lowest among the samples studied. These DSC−TG results jointly demonstrate that AlH_3 and CeF_3 have synergistic effects on the hydrogen desorption temperature of MgH_2.

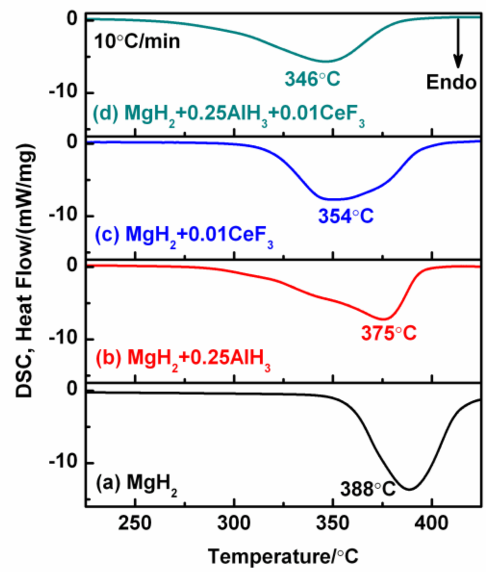

Fig. 1 DSC curves of the as-milled MgH_2 (a), MgH_2 + $0.25AlH_3$ (b), MgH_2 + $0.01CeF_3$ (c), and MgH_2 + $0.25AlH_3$ + $0.01CeF_3$ (d) samples.

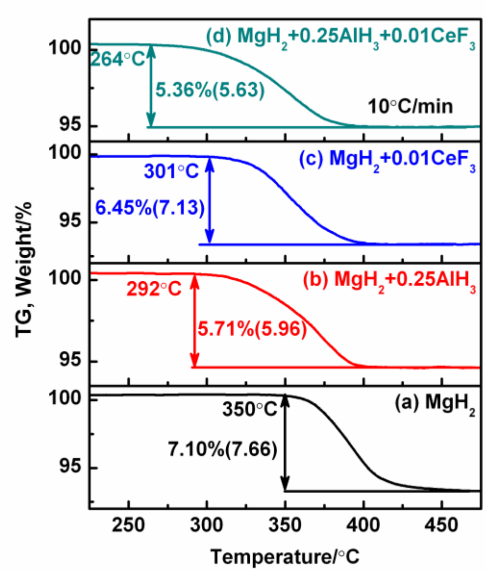

Fig. 2 TG curves of the as-milled MgH_2 (a), MgH_2 + $0.25AlH_3$ (b), MgH_2 + $0.01CeF_3$ (c), and MgH_2 + $0.25AlH_3$ + $0.01CeF_3$ (d) samples.

The hydrogen desorption kinetics of the samples are investigated by isothermal desorption at 300 °C and the fractional hydrogen desorption curves are displayed in Fig. 3. It is observed that the as-milled MgH_2 releases a very small amount of hydrogen after desorption at 300 °C for 3 h, which can also be confirmed by the XRD result of the desorption product in Fig. S2 (ESI†) that the majority of MgH_2 is still present in the desorption product. The hydrogen desorption of AlH_3-doped MgH_2 first accelerates for the initial 30 min and then slows down for the following stage. As for the CeF_3-doped MgH_2, the hydrogen desorption first undergoes an induction period for the initial 20 min and then proceeds with a fast kinetics. However, it is interesting that by co-addition of AlH_3 and CeF_3, the induction period is absent and the desorption goes on rapidly with a speed as high as that of the CeF_3-doped MgH_2. In addition, the hydrogen desorption extent of the co-doped MgH_2 is over 90%, which is the highest among the samples studied.

Fig. S2 (ESI†) shows the XRD patterns of the isothermal desorption product of each sample. The desorption product of the MgH_2 + $0.25AlH_3$ sample mainly contains $Mg_{17}Al_{12}$, Mg, and some un-decomposed MgH_2, while they are Mg and some trace of un-decomposed MgH_2 for the MgH_2 + $0.01CeF_3$ sample. However, no CeF_3-relevant phases are detected; this may be due to the low addition content of CeF_3. As for the MgH_2 + $0.25AlH_3$ + $0.01CeF_3$ sample, it mainly contains the $Mg_{17}Al_{12}$ and Mg phases and no un-decomposed MgH_2 is detected, suggesting that MgH_2 can fully decompose by co-addition of $0.25AlH_3$ and $0.01CeF_3$. A diffraction peak located at 2Theta = 27°–28° is suspected of belonging to the phase of $CeH_{2\sim3}$. Although the CeF_3-relevant phases cannot be detected right here, the XRD results at least give the information that only partial decomposition of MgH_2 occurs in either the AlH_3-doped or the CeF_3-doped MgH_2 samples, but it is almost full decomposition for MgH_2 co-doped with AlH_3 and CeF_3.

Combined the kinetics results with the structure analysis, we conclude that the co-addition of AlH_3 and CeF_3 also synergistically improves the desorption kinetics and the desorption extent of MgH_2.

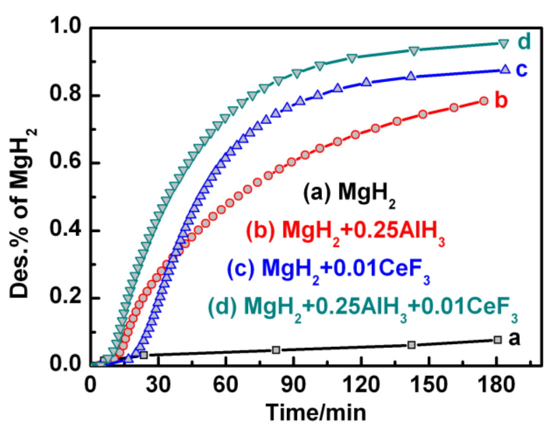

Fig. 3 Isothermal hydrogen desorption curves of as-milled samples plotted as fractional desorption of MgH_2 in the sample *vs.* time. The desorption temperature is 300 °C.

The cycling desorption properties of MgH_2 co-doped with AlH_3 and CeF_3 were studied by measuring the isothermal desorption curves at 300 °C for 10 cycles, which are shown in Fig. 4a. As can be seen that the desorption kinetics first accelerates at the second cycle and then is maintained for the following cycles. From Fig. 4b, it is shown that the capacity of 1-h desorption first increases for the initial 3 cycles and then is maintained at a value of *ca.* 3.6 wt% despite of a slight decrease at cycle 8. The capacity of 3-h desorption is mainly maintained at a value of *ca.* 4.5 wt%. These cycling desorption measurements indicate that the cycling desorption stability is extremely good for MgH_2 co-doped with AlH_3 and CeF_3.

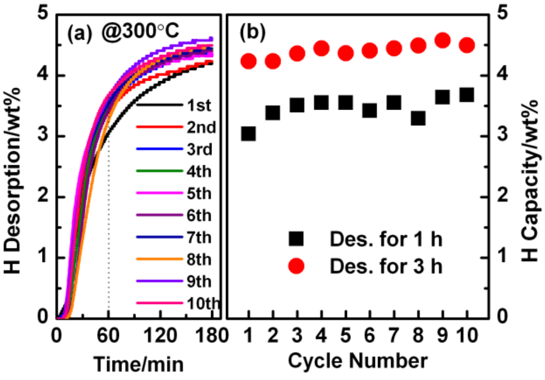

Fig. 4 (a) Cycling isothermal desorption curves of the MgH_2 + $0.25AlH_3$ + $0.01CeF_3$ sample; (c) Capacity of hydrogen released from the MgH_2 + $0.25AlH_3$ + $0.01CeF_3$ sample after desorption for 1 h and 3 h respectively *vs.* cycle number. The desorption temperature is 300 °C.

It has been shown in Fig. S2 (ESI†) that due to low addition amount, we cannot detect any CeF_3-relevant phase by XRD either in the as-milled samples (Fig. S1) or in the desorption product (Fig. S2 (ESI†)). In order to facilitate the detection of the CeF_3-relevant phases using XRD technique, the content of CeF_3 was increased and two series of samples, *i.e.*, MgH_2 + $mCeF_3$ (m = 0.01, 0.02, and 0.05) and MgH_2 + $0.1AlH_3$ + $nCeF_3$ (n = 0.01, 0.02, and 0.05), were prepared by ball milling. Their XRD patterns are shown in Fig. S3 (ESI†). It can be seen that the as-milled samples are mainly the physical mixture of the starting materials. CeF_3 is detected in the as-milled samples (see Fig. S3d−i (ESI†)) and does not react with MgH_2 or AlH_3 during ball milling. The Scherrer's equation[33] was utilized to estimate the grain sizes of MgH_2 in the samples, which are indicated in the figure. The grains of MgH_2 can be refined from (43~44) nm to (38~40) nm by addition of $0.01CeF_3$ and further refinement to (25~28) nm can be achieved by addition of $0.05CeF_3$. That is to say, CeF_3 addition is likely to refine the grains of MgH_2.

The XRD patterns of the desorption product of MgH_2 + $0.1AlH_3$, MgH_2 + $0.05CeF_3$, AlH_3 + $0.1CeF_3$, and MgH_2 + $0.1AlH_3$ + $0.02CeF_3$ are presented in Fig. 5. The desorption product of the MgH_2 + $0.1AlH_3$ sample contains Mg, $Mg_{17}Al_{12}$, and un-decomposed MgH_2, which means that MgH_2 has reacted with Al to form $Mg_{17}Al_{12}$. There exist Mg, a small amount of un-decomposed MgH_2, MgF_2, and $CeH_{2\sim3}$ in the desorption product of the MgH_2 + $0.05CeF_3$ sample; this suggests that CeF_3 may have reacted with MgH_2 during desorption process to form MgF_2 and $CeH_{2\sim3}$. Then from the desorption product of the AlH_3 + $0.1CeF_3$ sample, it is indicated that AlH_3 prefer to decompose by itself and will not react with CeF_3 during desorption process since CeF_3 remains unreacted in the sample before and after desorption. As for the MgH_2 + $0.1AlH_3$ + $0.02CeF_3$ sample, it is seen that a mixture of Mg, $Mg_{17}Al_{12}$, MgF_2, $CeH_{2\sim3}$, and some trace of un-decomposed MgH_2 exist in the desorption product. These products suggest that on one hand, Al (formed from decomposition of AlH_3) will react with MgH_2 to form $Mg_{17}Al_{12}$; on the other hand, CeF_3 will also react with MgH_2 to form MgF_2 and $CeH_{2\sim3}$. From the inset in Fig. 5, it is observed that the diffraction peak of Mg in the desorption products of MgH_2+$0.1AlH_3$ or MgH_2 + $0.1AlH_3$ + $0.02CeF_3$ has shifted to higher angles, which indicates that some Al atoms have dissolved into the crystal structure of Mg and a Al-doped Mg solid solution (denoted as $Mg_{ss}(Al)$) is formed.

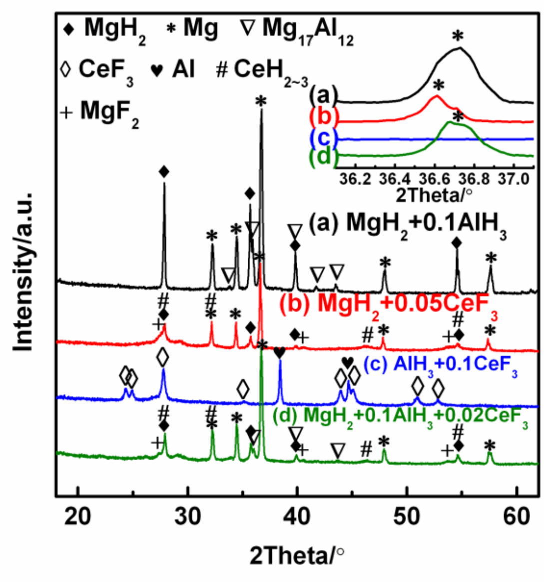

Fig. 5 XRD patterns of the desorption products of the selective samples. The hydrogen desorption measurements were carried out isothermally at 300 °C for 3 h.

Based on the above phase analysis on the desorption product of each sample, we can conclude that after hydrogen desorption process, Al (formed from the decomposition of AlH_3) has reacted with MgH_2 forming Mg solid solution (Mg_{ss}(Al)) and $Mg_{17}Al_{12}$ according to Eqns. (2) and (3):

$$MgH_2 + Al^* \rightarrow Mg_{ss}(Al) + H_2 \qquad (2)$$

$$MgH_2 + Al^* \rightarrow Mg_{17}Al_{12} + H_2 \qquad (3)$$

Meanwhile, CeF_3 has reacted with MgH_2 forming MgF_2 and $CeH_{2\sim3}$ following Eq. (4). $CeH_{2\sim3}$ is a nonstoichiometric metal hydride.

$$MgH_2 + CeF_3 \rightarrow MgF_2 + CeH_{2\sim3} \qquad (4)$$

The formations of Mg solid solution and $Mg_{17}Al_{12}$ indicate that the thermal stability of MgH_2 may have been reduced by addition of AlH_3 since several theoretical studies have reported the stability of MgH_2 can be changed by doping with Al. Shang *et al.*[7] used first-principles calculations to study the stability of MgH_2 by metal doping and found that the formation heat of MgH_2 can be reduced from −75.99 kJ mol^{-1} H_2 for pure MgH_2 to −28.36 kJ mol^{-1} H_2 for MgH_2 doped with 20 mol% Al. Another theoretical calculation by Kelkar *et al.*[15] showed a reduction of 9.3 kJ mol^{-1} H_2 for the heat of formation of MgH_2 with addition of 6.25 mol% Al. The $Mg_{17}Al_{12}$ alloy was reported to have better hydrogen desorption/absorption properties than the pure Mg/MgH_2 materials. Bouaricha *et al.*[5] prepared $Mg_{17}Al_{12}$ alloy by ball milling the elemental Mg and Al. They found that $Mg_{17}Al_{12}$ shows improved hydrogen sorption properties than the pure Mg and can be reversibly hydrided into MgH_2 and Al under conditions of 400 °C and 38 bar H_2. It was ascertained that the hydrogenation of $Mg_{17}Al_{12}$ proceeds in two steps[5, 34, 35]. At first, $Mg_{17}Al_{12}$ is hydrided into Mg_2Al_3 and MgH_2. Then, Mg_2Al_3 is further hydrided into MgH_2 and Al in the second step. These reactions are totally reversible. Crivello *et al.*[35] demonstrated that the presence of Al in the $Mg_{17}Al_{12}$ materials leads to an increase of their plateaus pressure, which means that Al can destabilize MgH_2 by forming the Mg−Al alloys. Therefore, MgH_2 has been thermodynamically destabilized by AlH_3 in the present work and this may contribute to the absence of the induction period in the isothermal desorption curves of AlH_3-doped MgH_2 in Fig. 3. As the isothermal desorption was carried out by quickly heating the sample to 300 °C (within 10−15 min) followed by holding at this temperature, which is very close to the practical heating condition, the destabilized AlH_3-doped MgH_2 can start to release hydrogen at a lower temperature than MgH_2 without AlH_3 addition, which results in the absence of the induction period.

With respect to the formation of MgF_2, it was suggested MgF_2 may benefit the initial activation of MgH_2 during the hydrogen desorption process.[36] As for the $CeH_{2\sim3}$, some literatures have reported the formation of this rare earth hydride from either the as-milled MgH_2−Ce composite or the hydrogenation product of Mg−Ni−Ce alloys.[12, 27, 37, 38] However, the $CeH_{2\sim3}$ in our present work is generated from the reaction between MgH_2 and CeF_3. The transition metal fluorides like CeF_3 are generally very fine, which will lead to more uniform distribution of $CeH_{2\sim3}$ on the particle surfaces or the grain boundaries of MgH_2. $CeH_{2\sim3}$ may act as a "hydrogen pump", which helps deliver hydrogen atoms from/to the MgH_2/Mg matrix during hydrogen desorption-absorption process, thus improving the hydrogen sorption kinetics of MgH_2 as shown in Fig. 3. On the other hand, $CeH_{2\sim3}$/MgF_2 layers can also serve as the impediment to the grain growth or coarsing of MgH_2 during cycling sorption process. These two factors are the main cause of the improvement of the desorption kinetics (Fig. 3) and the extremely good cycling stability (Fig. 4) of MgH_2.

A schematic diagram displaying the structure evolutions of AlH_3 and CeF_3 during the sample preparation and the hydrogen desorption process can be seen in Fig. S4 (ESI†). A briefly description of the evolutions is given below. Firstly, the MgH_2−AlH_3−CeF_3 composite is prepared by ball milling the starting materials of MgH_2, AlH_3 and CeF_3. After milling, the particle sizes of the starting materials will decrease because both the two hydrides are brittle materials, Meanwhile, CeF_3 may cover on the surfaces of the particles of MgH_2 and AlH_3. MgH_2 and AlH_3 particles will also contact closely with each other after milling. Then during the hydrogen desorption process (i.e. at the heating stage), AlH_3 will firstly decompose to form the oxide-free Al* and this freshly formed Al* will further react with MgH_2 to form the Mg solid solution (Mg_{ss}(Al)) and $Mg_{17}Al_{12}$, thus thermodynamically improving the desorption properties of MgH_2. On the other side, CeF_3 will also react with MgH_2 to form MgF_2 and $CeH_{2\sim3}$, which distribute surrounding the particles of Mg-Al phases and act both as the impediment to the grain growth of Mg-Al phases and as the hydrogen diffusion gateways. In this way, the MgF_2/$CeH_{2\sim3}$ layers can kinetically improve the desorption properties of MgH_2. In a word, this schematic diagram delivers a picture on how the thermodynamics and the kinetics of MgH_2 are tailored by co-addition of AlH_3 and CeF_3. The synergistic effect is believed to contribute to the reduction of desorption temperature, the absence of desorption induction period, the acceleration of desorption kinetics and the extremely good cycling stability.

Finally, we carried out the thermal decompositions of the MgH_2 + $m$$CeF_3$ and the MgH_2 + 0.1AlH_3 + $n$$CeF_3$ samples by DSC analysis, which are shown in Fig. 6. It is found in Fig. 6a−c that the peak desorption temperatures of the MgH_2 + $m$$CeF_3$ samples generally locate at about 360 °C even if the CeF_3 addition is increased. A study by Jin *et al.* also showed that the desorption temperature of MgH_2 doped with 1 mol% CeF_3 is only slightly reduced by less than 20 °C; this reduction is even less than our present work (about 30 °C). However, it is seen from Fig. 6d−f that in the presence of 0.1AlH_3, the peak desorption temperature of MgH_2 can be further reduced if the CeF_3 addition is increased. A reduction of about 70 °C is achieved for the MgH_2 + 0.1AlH_3 + 0.05CeF_3 sample compared to the pure MgH_2 in Fig. 1a.

To preliminarily study the role of AlH_3 in the MgH_2 + 0.1AlH_3 + 0.05CeF_3 sample, we carried out morphology analysis on the as-milled MgH_2 with or without AlH_3 addition. Fig. 7 shows the SEM images of the pure MgH_2 sample and the MgH_2 + 0.25AlH_3 sample after ball milling. It is seen that the particles of the as-milled MgH_2 + 0.25AlH_3 sample are generally smaller than that of the as-milled pure MgH_2 sample, which suggests that AlH_3 addition will lead to particle refinement of MgH_2. This may imply that more MgH_2 particle surfaces will contact with the excess CeF_3. More closely contacting means that more MgF_2/$CeH_{2\sim3}$ phases acting as hydrogen diffusion gateways will be generated, thus further reducing the desorption temperature of MgH_2. It should be noted that this temperature reduction may origin from the kinetic enhancement rather than the destabilization effect. As the hydrogen desorption analysis of the samples were carried out by DSC measurements with a relatively fast heating rate of 10 °C/min. Such a heating rate may lead to hysteresis in the DSC curves if the reaction kinetics is not fast enough. The AlH_3-added Mg-based material may possesses more MgF_2/$CeH_{2\sim3}$ phases acting as hydrogen diffusion gateways, thus behaving better kinetic properties. Therefore, the AlH_3 addition in our present work was believed to kinetically help CeF_3 to take effect on the Mg-based materials. All in all, in addition to thermodynamically destabilizing MgH_2, AlH_3 may also kinetically help CeF_3 to take effect on the MgH_2. However, the exact role of AlH_3 should be carefully studied in detail by other analysis techniques.

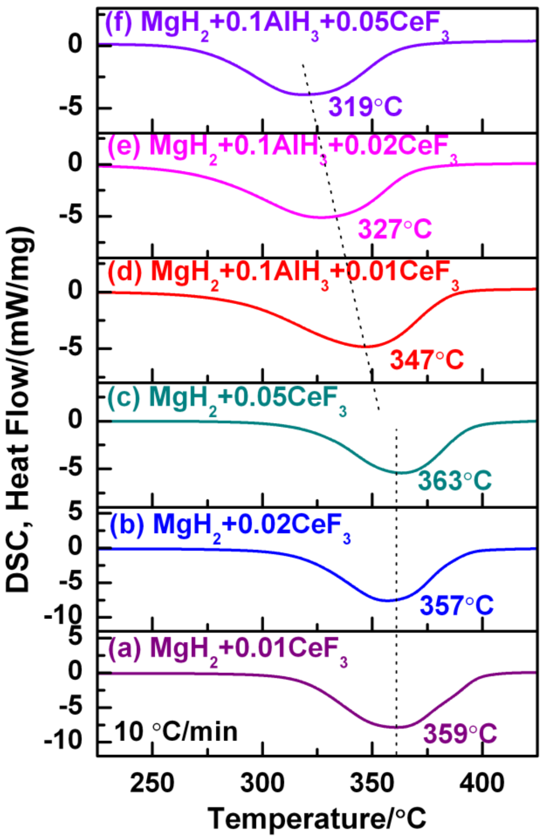

Fig. 6 DSC curves of MgH_2 + $m$$CeF_3$ (m = 0.01, 0.02, and 0.05) (a-c) and MgH_2 + 0.1AlH_3 + $n$$CeF_3$ (n = 0.01, 0.02, and 0.05) (d-f) samples.

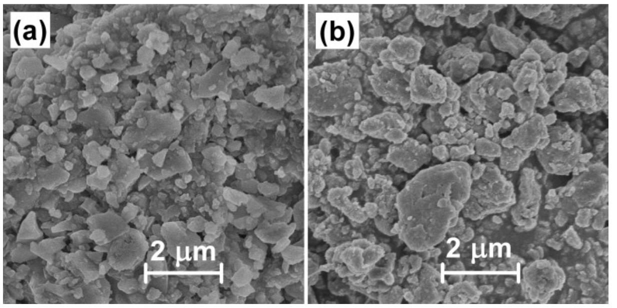

Fig. 7 SEM images of the as-milled samples: (a) MgH_2 + 0.25AlH_3; (b) MgH_2.

Conclusions

The hydrogen desorption properties, involving the kinetics, the thermodynamics, and the cycling stability of MgH_2 is significantly improved by synergistic addition of AlH_3 and CeF_3. The formations of Mg solid solution and $Mg_{17}Al_{12}$ contribute to the thermodynamic destabilization of MgH_2, while the formation of $CeH_{2\sim3}$ acting as "hydrogen pump" and impediment to grain growth of MgH_2 leads to the improvement of the kinetics and the extremely good cycling stability of MgH_2. Finally, it was found AlH_3 would kinetically help CeF_3 to take effect on MgH_2. This work provides a method for simultaneously tailoring the thermodynamic and kinetic properties of MgH_2 by synergistic addition of metal hydride and rare earth fluoride.

Acknowledgements

This work was supported by the National Natural Science Foundation of China (NO. 51171168 and 51471149), Public Project of Zhejiang Province (NO. 2013C31033), Key Science and Technology Innovation Team of Zhejiang province (NO. 2010R50013), and Program for Innovative Research Team in University of Ministry of Education of China (IRT13037).

Notes and References

† Electronic Supplementary Information (ESI) available: Fig. S1−S4. See DOI: 10.1039/c000000x/

[a] State Key Laboratory of Silicon Materials, School of Materials Science and Engineering, Zhejiang University, Hangzhou 310027, China.
[b] Zhejiang Metallurgical Research Institute, Hangzhou 310017, China.
[c] Key Laboratory of Advanced Materials and Applications for Batteries of Zhejiang Province, Zhejiang University, Hangzhou 310027, China.
[*] Corresponding authors:
(a) E-mail: xinhwang@zju.edu.cn (X.H. Wang), Tel/Fax: +86-571-87952716.
(b) E-mail: chen_wu@zju.edu.cn (C. Wu).

1. P. Selvam, B. Viswanathan, C. S. Swamy and V. Srinivasan, *Int. J. Hydrogen Energy*, 1986, **11**, 169-192.
2. K. F. Aguey-Zinsou and J. R. Ares-Fernandez, *Energy Environ. Sci.*, 2010, **3**, 526-543.

3. F. Cheng, Z. Tao, J. Liang and J. Chen, *Chem. Commun.*, 2012, **48**, 7334-7343.
4. A. Zaluska, L. Zaluski and J. O. Strom-Olsen, *J. Alloys Compd.*, 1999, **289**, 197-206.
5. S. Bouaricha, J. P. Dodelet, D. Guay, J. Huot, S. Boily and R. Schulz, *J. Alloys Compd.*, 2000, **297**, 282-293.
6. G. Liang, J. Huot, S. Boily, A. Van Neste and R. Schulz, *J. Alloys Compd.*, 1999, **292**, 247-252.
7. C. X. Shang, M. Bououdina, Y. Song and Z. X. Guo, *Int. J. Hydrogen Energy*, 2004, **29**, 73-80.
8. C. S. Zhou, Z. G. Z. Fang, J. Lu and X. Y. Zhang, *J. Am. Chem. Soc.*, 2013, **135**, 10982-10985.
9. P. Kalisvaart, E. Luber, H. Fritzsche and D. Mitlin, *Chem. Commun.*, 2011, **47**, 4294-4296.
10. J. Yuan, Y. Zhu and L. Li, *Chem. Commun.*, 2014, **50**, 6641-6644.
11. J. Cui, H. Wang, J. Liu, L. Ouyang, Q. Zhang, D. Sun, X. Yao and M. Zhu, *J. Mater. Chem. A*, 2013, **1**, 5603-5611.
12. J. Cui, J. Liu, H. Wang, L. Ouyang, D. Sun, M. Zhu and X. Yao, *J. Mater. Chem. A*, 2014, **2**, 9645-9655.
13. G. Xin, J. Yang, H. Fu, W. Li, J. Zheng and X. Li, *RSC Advances*, 2013, **3**, 4167-4170.
14. Y. Liu, J. Zou, X. Zeng and W. Ding, *RSC Advances*, 2014, **4**, 42764-42771.
15. T. Kelkar and S. Pal, *J. Mater. Chem.*, 2009, **19**, 4348-4355.
16. J. H. Dai, Y. Song and R. Yang, *Int. J. Hydrogen Energy*, 2011, **36**, 12939-12949.
17. A. Zaluska, L. Zaluski and J. O. Strom-Olsen, *Appl. Phys. A: Mater. Sci. Process.*, 2001, **72**, 157-165.
18. H. Z. Liu, X. H. Wang, Y. A. Liu, Z. H. Dong, G. Z. Cao, S. Q. Li and M. Yan, *J. Mater. Chem. A*, 2013, **1**, 12527-12535.
19. H. Z. Liu, X. H. Wang, Y. G. Liu, Z. H. Dong, H. W. Ge, S. Q. Li and M. Yan, *J. Phys. Chem. C*, 2014, **118**, 37-45.
20. H. Z. Liu, X. H. Wang, Y. A. Liu, Z. H. Dong, S. Q. Li, H. W. Ge and M. Yan, *J. Phys. Chem. C*, 2014, **118**, 18908-18916.
21. S. A. Jin, J. H. Shim, Y. W. Cho and K. W. Yi, *J. Power Sources*, 2007, **172**, 859-862.
22. J. W. Kim, J. P. Ahn, S. A. Jin, S. H. Lee, H. S. Chung, J. H. Shim, Y. W. Cho and K. H. Oh, *J. Power Sources*, 2008, **178**, 373-378.
23. A. Grzech, U. Lafont, P. C. Magusin and F. M. Mulder, *J. Phys. Chem. C*, 2012, **116**, 26027-26035.
24. I. E. Malka, T. Czujko and J. Bystrzycki, *Int. J. Hydrogen Energy*, 2010, **35**, 1706-1712.
25. I. E. Malka, M. Pisarek, T. Czujko and J. Bystrzycki, *Int. J. Hydrogen Energy*, 2011, **36**, 12909-12917.
26. M. Ismail, N. Juahir and N. S. Mustafa, *J. Phys. Chem. C*, 2014, **118**, 18878-18883.
27. M. Ismail, *Int. J. Hydrogen Energy*, 2014, **39**, 2567-2574.
28. M. Ismail, Y. Zhao, X. B. Yu and S. X. Dou, *RSC Advances*, 2011, **1**, 408-414.
29. M. F. Abdul Halim Yap, N. S. Mustafa and M. Ismail, *RSC Advances*, 2014.
30. F. M. Brower, N. E. Matzek, P. F. Reigler, H. W. Rinn, C. B. Roberts, D. L. Schmidt, J. A. Snover and K. Terada, *J. Am. Chem. Soc.*, 1976, **98**, 2450-2453.
31. H. Z. Liu, X. H. Wang, Y. A. Liu and M. Yan, *Chem. J. Chin. Univ.*, 2013, **34**, 2274-2278.
32. H. Z. Liu, X. H. Wang, Z. H. Dong, G. Z. Cao, Y. A. Liu, L. X. Chen and M. Yan, *Int. J. Hydrogen Energy*, 2013, **38**, 10851-10856.
33. L. Birks and H. Friedman, *J. Appl. Phys.*, 1946, **17**, 687-692.
34. Q. A. Zhang and H. Y. Wu, *Mater. Chem. Phys.*, 2005, **94**, 69-72.
35. J. C. Crivello, T. Nobuki, S. Kato, M. Abe and T. Kuji, *J. Alloys Compd.*, 2007, **446**, 157-161.
36. F. J. Liu and S. Suda, *J. Alloy. Compd.*, 1995, **231**, 742-750.
37. C. X. Shang and Z. X. Guo, *Int. J. Hydrogen Energy*, 2007, **32**, 2920-2925.
38. L. Z. Ouyang, X. S. Yang, M. Zhu, J. W. Liu, H. W. Dong, D. L. Sun, J. Zou and X. D. Yao, *J. Phys. Chem. C*, 2014, **118**, 7808-7820.